Vietnam Journal of Science and Technology ***63*** *(4) (2025) 734-744*

doi:10.15625/2525-2518/18013

Composition distribution and photoluminescence properties of colloidal Cu - doped $Zn_{0.5}Cd_{0.5}S$ quantum dots

Nguyen Dieu Linh[1], Nguyen Thi Minh Hien[2], Nguyen Thi Thuy Lieu[3], Tran Thi Kim Chi[4], Nguyen Xuan Nghia[2, *]

[1]*University of Science and Technology of Hanoi, 18 Hoang Quoc Viet, Cau Giay, Ha Noi, Viet Nam*

[2]*Institute of Physics, Vietnam Academy of Science and Technology, 18 Hoang Quoc Viet, Cau Giay, Ha Noi, Viet Nam*

[3]*Posts and Telecommunications Institute of Technology, km10 Nguyen Trai, Ha Noi, Viet Nam*

[4]*Institute of Materials Science, Vietnam Academy of Science and Technology, 18 Hoang Quoc Viet, Cau Giay, Ha Noi, Viet Nam*

[*]Emails: *nxnghia@iop.vast.vn*

Received: 4 January 2023; Accepted for publication: 15 May 2023

Abstract. This study aims to find a solution for preparing Cu-doped colloidal $Zn_{0.5}Cd_{0.5}S$ quantum dots (QDs) with different radial Zn and Cd composition distributions and investigate the effects of these distributions on the QDs' optical properties. QDs were prepared with a radial gradient composition distribution by rapidly and simultaneously injecting precursor solutions of Zn and Cd into the reaction flask. In contrast, QDs with a homogeneous composition distribution were prepared by injecting small amounts of Zn and Cd precursors alternately after the crystal nuclei had been formed, followed by thermal annealing of the QDs in the reaction solution. Cu doping $Zn_{0.5}Cd_{0.5}S$ QDs decreases their band edge luminescence and significantly increases their broad emission band at lower energy. This emission band is generated by radiative recombination related to the Cu dopant, as well as lattice defects such as interstitial atoms and vacancies. Different composition distributions do not affect the excitation power dependence behavior of band edge luminescence and dopant related emission intensities; however, they cause strong band gap energy renormalizations in Cu-doped ternary QDs with increasing excitation power density. This enhancement is attributed to the optically active region in small gradient alloyed QDs and the existence of a wetting layer surrounding it.

Keywords: Colloidal Cu-doped ZnCdS quantum dot, composition distribution, radiative transition, band gap energy renormalization.

Classification numbers: 2.1.1, 2.4.1.

1. INTRODUCTION

Ternary semiconductor nanomaterials are of great interest due to their prospective applications in electron confinement structures, photovoltaic heterojunction, creation of p-n junctions for window materials [1], and electro-optical devices [2]. Different from binary II-VI semiconductor compounds, ternary II-VI semiconductor nanomaterials' optical properties can be controlled not only by changing the particle size and morphology but also by changing their composition contents and composition distribution [3]. Besides, these nanomaterials are typically used as hosts for doping Cu, owing to their widely tunable emission wavelength and self-absorption minimization effect [4]. Doping transition metals in these materials creates dopant states in the band gap, changing their radiative transition mechanism, thus extending their applications in photonic and optoelectronics technologies [5, 6]. In recent years, much research has been performed on Cu-doped ternary II-VI semiconductor quantum dots (QDs) to clarify a number of issues, including oxidation states of Cu (Cu(I) and Cu(II)) in doped QDs [7], the exact position of Cu dopant's d energy level between the host semiconductor's valence and conduction bands [8], the relation between Cu doping viability and the host lattice's crystal structure [9, 10], and the effect of Cu doping on the host QDs' optical band gap energy [11, 12].

However, the differentiation between Cu dopant emission and the surface state emission of host semiconductor QDs is rarely mentioned in previous publications. These emission bands overlap and create a broad emission band at lower energies than that of the band edge emission peak [13]. In the case of Cu-doped binary II-VI semiconductor QDs, the similarities in these emission bands' position and full width at half maximum (FWHM) make differentiation between them difficult. This matter is further complicated in Cu-doped ternary II-VI semiconductor QDs since in addition to surface and dopant states, the host lattice often includes structural native defects such as interstitial atoms and vacancies [14]. Another subject, which is largely unresearched to our knowledge, is the effect of Cu-doped ternary II-VI semiconductor QDs' radial composition distributions on their optical properties. Depending on reaction conditions, these QDs may have different radial composition distributions (gradient [15] or homogeneous [14,16]), which affects their band gap energy structure, and as a consequence, their optical properties.

This study aims to identify the effect of different radial composition distributions on the photoluminescence (PL) properties of colloidal Cu-doped $Zn_{0.5}Cd_{0.5}S$ and establish their optical transition mechanism. 1 % Cu-doped $Zn_{0.5}Cd_{0.5}S$ QDs were prepared using the colloidal method. For comparison, their undoped counterparts were also prepared with the same reaction parameters. Different radial composition distributions in undoped and Cu-doped QDs were obtained by varying the precursor injection method and reaction time. Sample characteristics such as morphology, size, contents, crystal structure, and optical properties were investigated with transmission electron microscopy (TEM), energy dispersive X-ray (EDX), X-ray diffraction (XRD), UV-Vis absorption, and PL. The effect of different composition distributions on Cu-doped QDs' PL properties were analyzed based on excitation power dependent PL spectra with excitation power ranging from 0.6 to 600 mW/cm^2. Cu dopant emission was identified by comparing the low energy emission band of undoped and Cu-doped QDs, combined with our previous research on luminescence centers in undoped ZnCdS QDs.

2. MATERIALS AND METHODS

2.1. Materials

Initial chemicals including zinc stearate ($ZnSt_2$, 98 %) cadmium oxide (CdO, 99.5 %), copper chloride ($CuCl_2$, 97 %), tetramethylammonium hydroxide pentahydrate (97 %), sulfur powder (S, 99.98 %), stearic acid (SA, 95 %), and 1-octadecene (ODE, 90 %) were purchased from Aldrich and used as received without further purifications.

2.2. Preparation of Cu - doped $Zn_{0.5}Cd_{0.5}S$ quantum dots with gradient and homogenous composition distribution

1 % Cu-doped $Zn_{0.5}Cd_{0.5}S$ QD samples with gradient and homogeneous radial composition distribution (labeled as ACu and BCu respectively) were prepared using the colloidal method with hot injection. The ACu sample was retrieved by rapidly and simultaneously injecting precursor solutions of Zn, Cd, and Cu into the S precursor solution heated to 280 ℃, and letting them react for 15 min. The preparation of the BCu sample consists of two stages. In the first stage, a mixture of all the Cu precursor solution and 20 % of the Zn and Cd precursor solutions was rapidly injected into the S precursor solution heated to 280 ^oC to create crystal nuclei. Then, small amounts of the remaining Zn and Cd precursor solutions were injected into the reaction solution in an alternating manner, with the duration between two consecutive injections of 3 min. After this stage, which was performed for approximately 30 min, the QDs were annealed for 240 min in the reaction solution at 280 ^oC. The precursor solutions and QD samples were prepared in a pure (99.999 %) nitrogen gas environment.

As known, the reaction speed of Cd-S is higher than that of Zn-S. Therefore, the rapid and simultaneous injection of the Zn and Cd precursors into the S precursor at reaction temperature typically creates ZnCdS QDs with a Cd-rich center and a Zn-rich outer region (QDs with gradient radial composition distribution) [15]. Preparing homogeneous composition distribution QDs using this method requires annealing them for long durations. Alternately injecting Zn and Cd precursor solutions into a S precursor and crystal nuclei solution creates Zn-rich and Cd-rich layers in the QDs, thus reducing the diffusion time of Zn and Cd atoms, allowing QDs with a homogeneous composition distribution to be created.

For comparison purposes, undoped $Zn_{0.5}Cd_{0.5}S$ QD samples with gradient and homogeneous composition distribution (labeled as A0 and B0 respectively) were also prepared in the same manner as the ACu and BCu samples.

After the preparation, undoped and Cu-doped QD samples were separated from their reaction solutions by first mixing the solution with isopropanol at a volume ratio of 1:5 and then centrifuging it at 1300 rpm for 3 min. Part of the QDs in powder form were used in XRD measurements, and the remaining portion were dispersed in toluene to investigate their morphology and spectroscopic characteristics.

2.3. Sample characterization

TEM images of the samples were recorded using the JEM 1010 microscope (Jeol). Powder XRD measurements were conducted with the D5005 X-ray diffractometer (Siemens) with Cu-K_α radiation wavelength of 0.15406 nm. The JSM 6490 microscope (Jeol) equipped with the JED 2300 analysis station (Jeol) was used to retrieve the samples' EDX spectra. UV-Vis absorption spectra were recorded using the Varian Cary-5000 spectrometer. To minimize reabsorption, samples with low QD concentrations in toluene were used. The PL and excitation power dependent PL measurements were performed with the irH550 spectrometer with the excitation

wavelength of 355 nm. The laser trace's diameter was approximately 1 mm. The excitation power density was changed in the range of 0.6 - 600 mW/cm^2 using filters.

3. RESULTS AND DISCUSSION

3.1. Morphology, composition, and crystal structure of Cu-doped $Zn_{0.5}Cd_{0.5}S$ quantum dots

As can be seen from the TEM images of the samples in Figure 1, the Cu-doped nanocrystals (NCs) have a spherical shape. The average diameters of the ACu and BCu QDs were determined as 5.2 and 7.7 nm respectively with approximately 300 particles using the ImageJ software. Carrier confinement in both QD types is weak due to the similarity of their radii with the Bohr exciton radii of ZnS and CdS (2.2 and 3 nm respectively [17]). The band gap energy is mostly determined by the Zn and Cd contents in this case. From the diameter distribution graphs, the BCu sample is shown to have a wider size distribution than that of the ACu sample, which is a result of the Ostwald ripening [18] phenomenon occurred when annealing the BCu sample for long periods to obtain a homogeneous composition distribution in the QDs. In addition to this unwanted consequence, Ostwald ripening also homogenizes the composition distribution in ternary QDs.

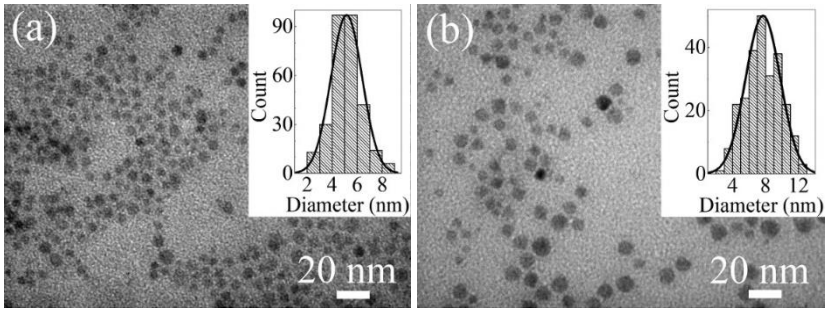

Figure 1. TEM images of the ACu (a) and BCu (b) samples.

Figure 2 presents the representative EDX spectrum of the undoped B0 sample. EDX analysis results listed in Table 1 show that the Zn and Cd contents in the sample match the calculated values for preparing the $Zn_{0.5}Cd_{0.5}S$ QDs within margins of error [19].

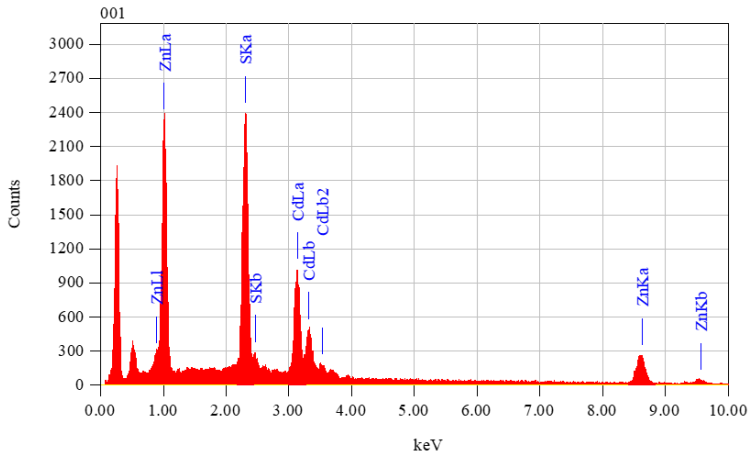

Figure 2. Representative EDX spectrum of the B0 sample.

Table 1. Results obtained from EDX analysis for the B0 sample.

Composition	Calculated values (at. %)	Average measured values (at. %)	Composition content
Zn	25	23.9	0.53
Cd	25	21.0	0.47
S	50	55.1	

From the XRD patterns shown in Figure 3, it can be concluded that the ACu and BCu samples both have a wurtzite (Wz) structure. The XRD pattern of the ACu sample is characterized by diffraction peaks at 26, 27.5, 29.5, 38.7, 45.6, 49.7, and 54.2°, corresponding to Miller indices (100), (002), (101), (102), (110), (103), and (112) of the Wz structure respectively (written as regular text in Figure 3(a)). Meanwhile, the BCu sample's diffraction peaks are slightly shifted towards smaller 2θ angles; specifically, they are located at 25.9, 27.4, 29.3, 38.1, 45.7, 49.4, and 54.1° (Figure 3(b)).

XRD pattern analysis results for the samples using the Voigt function show that the diffraction intensity ratios between the 26 and 27.5° peaks of the ACu and BCu samples are 0.49 and 0.41 respectively. Practically, the QD samples were treated as crystal samples in powder form. The intensity ratios between (100) and (002) diffraction peaks of Wz-ZnS and Wz-CdS samples according to JCPDS cards 36-1450 and 41-1049 are 1.19 and 0.68 respectively, higher than those determined from the obtained patterns, proving the simultaneous existence of both Wz and zinc blende (Zb) structural phases in the investigated samples. In Figure 3, the Zb phase's Miller indices were written in italics. As known, the Zb structure's light and heavy hole bands degenerated at the Brillouin zone's Γ point are separated in the Wz structure due to the crystal field [20]. However, it does not cause a significant change in the optical band gap energy of II-VI NCs [21].

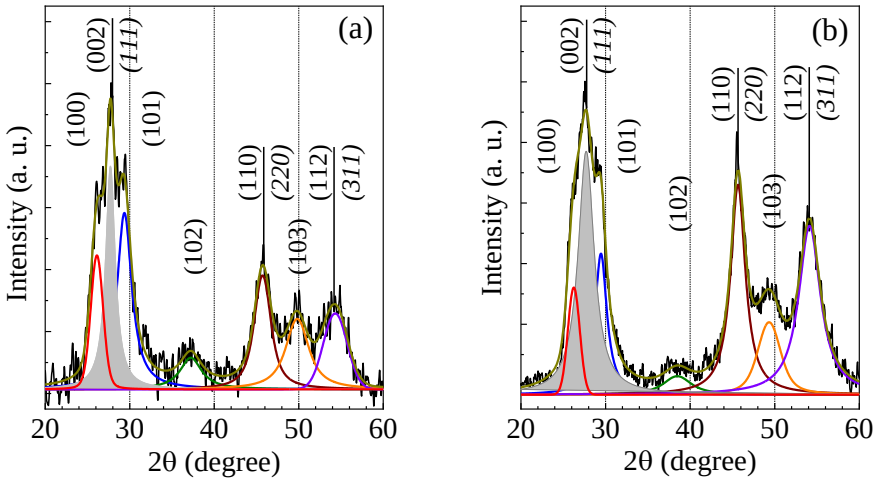

Figure 3. XRD patterns of the ACu (a) and BCu (b) samples. The diffraction peaks' positions were determined using the Voigt function. Miller indices of the Wz and Zb structural phases were shown in regular and italic digits respectively.

As previously mentioned in Section 2.2, injecting all the Cu precursor solution into the reaction solution at the beginning of the preparation process will allow for the complete doping of the QDs. However, different injection methods used for the ACu and BCu samples will lead

to different Zn and Cd distributions in these samples: gradient radial composition distribution with a Cd-rich center and Zn-rich outer region for the ACu sample, and homogeneous composition distribution for the BCu sample. As a result, the ACu sample's band gap structure differs from that of the BCu sample. As mentioned above, due to the weak carrier confinement, the band gap energies of the investigated samples are governed by the composition contents. The Cd-rich center region in ACu QDs has the lowest energy of $E_{g.A}$ (band gap energy), and the band gap width is expanded towards the QDs' surface. Therefore, carriers generated from photoexcitation are concentrated in this region. Meanwhile, radiative recombination will occur throughout the BCu QD due to its homogeneous composition distribution, and this QD type's $E_{g.B}$ band gap energy is higher than the $E_{g.A}$.

3.2. Optical transitions in Cu-doped $Zn_{0.5}Cd_{0.5}S$ quantum dots

UV-Vis absorption and PL spectra of undoped and Cu-doped sample pairs (A0, ACu) and (B0, BCu) are compared in Figure 4. The samples' first exciton absorption peak's energy positions were determined at the second-order derivative minima of the absorption spectra and are 2.90, 2.89, 2.94, and 2.95 eV for the A0, ACu, B0, and BCu samples respectively. The blue shift of the B0 and BCu samples' first exciton absorption peak compared to the A0 and ACu samples are caused by the former's higher band gap energy compared to that of the latter.

To verify the homogeneity of the Zn and Cd distribution in BCu QDs, their optical band gap energy was compared with the theoretical band gap energy. As mentioned above, their band gap energy can be compared with that of bulk $Zn_{0.5}Cd_{0.5}S$ due to the weak carrier confinement in ACu and BCu QDs. As known, the band gap energy of bulk $Zn_xCd_{1-x}S$ with heterogeneous composition distribution ($E_{g.bulk}^{Zn_xCd_{1-x}S}$) is dependent on the Zn content (x) and is described by the below expression [14]:

$$E_{g.bulk}^{Zn_xCd_{1-x}S} = xE_{g.bulk}^{ZnS} + (1-x)E_{g.bulk}^{CdS} - bx(1-x)$$

with $E_{g.bulk}^{ZnS}$ = 3.7 eV and $E_{g.bulk}^{CdS}$ = 2.5 eV [22] being the band gap energies of bulk ZnS and CdS respectively, and b = 0.61 being the size-independent optical bowing constant for $Zn_xCd_{1-x}S$ NCs [14, 23]. The bulk $Zn_xCd_{1-x}S$ band gap energy has been calculated to be 2.957 eV with x = 0.5, close to the optical band gap energies determined from the B0 and BCu QDs' UV-Vis absorption spectra, and far from those of the A0 and ACu QDs. This evidence proved that the Zn and Cd composition distribution is homogeneous in the B0 and BCu QDs, and gradient in the A0 and ACu QDs.

The samples' PL spectra include band edge luminescence peaks P_{BE} at high energy and broad emission bands at lower energy levels. The P_{BE} peak positions for the A0, ACu, B0, and BCu samples are 2.77, 2.78, 2.80, and 2.84 eV respectively. Notably, Cu doping not only greatly increases the low energy emission band intensity but also broadens it towards longer wavelengths.

As can be seen in Figure 4, the behavior of the low energy emission band exhibits the appearance of different radiative recombination transition mechanisms. To determine these mechanisms, the PL spectra of the samples were analyzed using Gaussian and Lorentzian distribution convolution. The obtained results demonstrated that the A0 and B0 samples' emission bands consist of two component luminescence peaks at approximately 2.2 and 2.0 eV (labeled as P1 and P2 respectively).

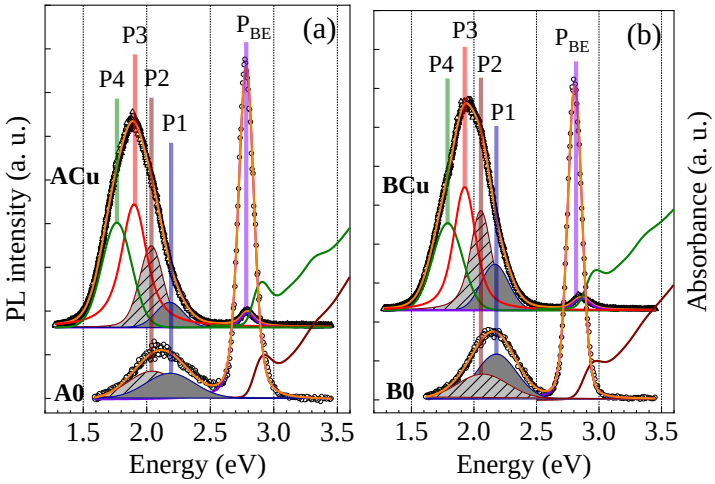

Figure 4. Comparison of UV-Vis absorption and PL spectra of the A0 and ACu (a), and B0 and BCu (b) samples. For clarity, the absorption and PL spectra of the ACu and BCu samples were shifted upwards.

Based on our previous research on luminescence centers in colloidal $Zn_xCd_{1-x}S$ QDs via synchronous luminescence spectroscopy [19], P1 is attributed to the recombination of carriers between sulfur vacancy V_S related donor level and the valence band edge, and P2 is attributed to the radiative transition from interstitial zinc/cadmium (I_{Zn}/I_{Cd})-related donor level to zinc/cadmium vacancy (V_{Zn}/V_{Cd})-related acceptor level. The low energy emission bands of the ACu and BCu samples are better described by four component luminescence peaks. Along with P1 and P2 peaks in the 2.0-2.2 eV region, the appearance of two other peaks at 1.9 and 1.75 eV (labeled as P3 and P4 respectively) causes the broadening of this band towards longer wavelengths. P3 is attributed to the radiative recombination transition from the conduction band's ground state to the Cu^{2+} ion's T_2 level, and P4 is caused by the optical transition from I_{Cd}/I_{Zn} and V_S levels to the T_2 level as illustrated in Figure 5.

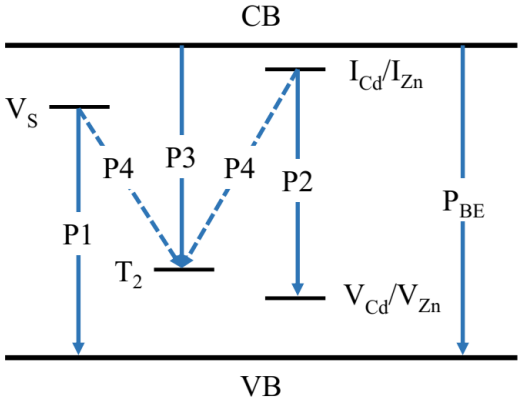

Figure 5. Schematic diagram of the radiative recombination between energy levels in the ACu and BCu samples.

3.3. Excitation power dependent photoluminescence of Cu-doped $Zn_{0.5}Cd_{0.5}S$ quantum dots having different composition distributions

Figure 6 presents the excitation power dependent PL spectra of the ACu and BCu samples. The rise of excitation power density from 0.6 to 600 mW/cm^2 causes a strong increase in the PL intensity and the red shift of the band edge luminescence peak P_{BE}. As can be seen from Figure 7(a), as the excitation power density increases from 0.6 to 600 mW/cm^2, the P_{BE} peak of the ACu and BCu samples were red shifted by 28 meV and 3 meV respectively. This phenomenon is caused by band gap energy renormalization as the carrier concentration increases [24]. This renormalization occurs more significantly in the ACu sample compared to the BCu sample and is explained to be the result of a smaller optically active region (which can be defined as the Cd-rich region), as well as the surrounding of this region by a Zn-rich wetting layer [25].

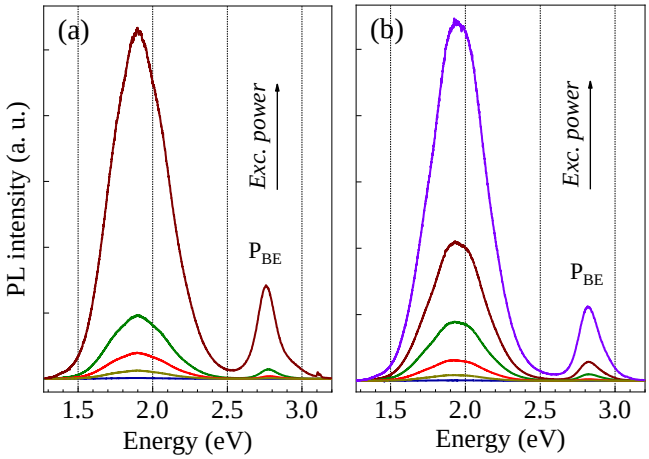

Figure 6. Excitation power dependent PL spectra of the ACu (a) and BCu (b) samples.

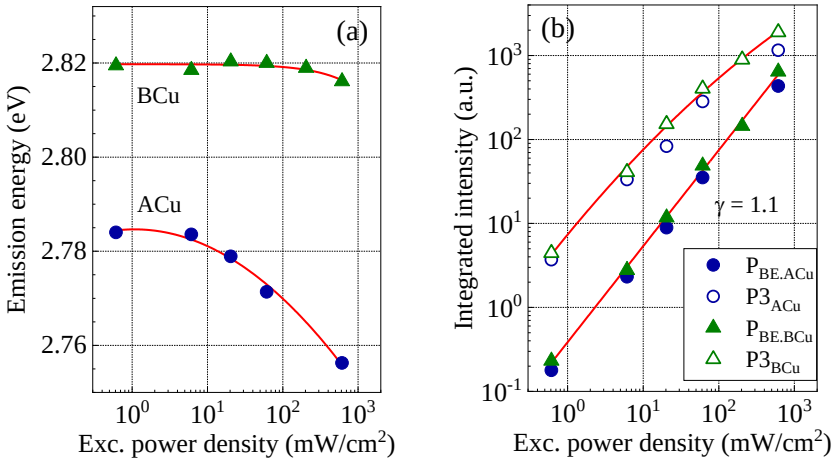

Figure 7. Band edge emission energy (a), and integrated emission intensity of P_{BE} and P3 peaks (b) of the ACu and BCu samples as functions of excitation power density. The solid lines show the trends of the emission energy (Figure 7(a)) and integrated emission intensity (Figure 7(b)) as the excitation power density is changed.

Figure 7(b) demonstrates the dependence of the P_{BE} and P3 peaks' integrated emission intensity on excitation power density in the ACu and BCu samples. As known, the luminescence intensity (I)'s dependence on excitation power (p) is described as $I \sim p^{\gamma}$. It can be seen from the

figure that $\gamma \sim 1$ leads to a linear increase in P_{BE} intensity of both samples in the 0.6 - 600 mW/cm^2 range. In contrast, deviation from this linearity were observed in both samples' P3 peak, reflecting the competition between carrier recombination channels in Cu-doped QD samples.

4. CONCLUSIONS

Cu-doped $Zn_{0.5}Cd_{0.5}S$ QDs with different radial Zn and Cd composition distributions were prepared using the colloidal method at 280 ℃. QDs with a core/shell structure having the Cd-rich center and Zn-rich outer region (the ACu sample) were prepared by rapidly and simultaneously injecting all the Zn, Cd and Cu precursor solutions into the S precursor solution heated to reaction temperature. In contrast, QDs with homogeneous composition distribution (the BCu sample) were obtained by alternately injecting small amounts of Zn and Cd precursors into the reaction solution after creating crystal nuclei, followed by thermal annealing of the QDs in the reaction solution for 240 min.

The ACu and BCu QDs have an average diameter of 5.2 and 7.7 nm respectively, and a crystal structure consisting of Wz and Zb phases. Cu doping greatly increases the broad low energy emission band's intensity. This band is generated mainly due to recombination transitions related to the Cu dopant, and lattice defects such as interstitial Zn and Cd atoms and Zn, Cd and S vacancies. Comparison of PL characteristics of the ACu and BCu samples with different Zn and Cd composition distributions demonstrated that the behaviors of the band edge luminescence peak intensity and emission intensity caused by transition between the conduction band's ground state and the Cu^{2+} ion's T_2 level are similar in both samples in the excitation power density range of 0.6 - 600 mW/cm^2. However, the radial gradient composition distribution in ACu QDs causes a strong renormalization of their band gap energy. The enhancement of this effect in core/shell nanostructures is attributed to the increase in carrier concentrations in smaller optically active regions and the existence of a wetting layer on the ACu QDs' surface.

The achieved results not only provide a solution for actively controlling the composition distribution of transition metal doped ternary QDs, but also shows the relationship between their PL characteristics and their band gap structure, which is useful for the practical applications of these materials.

Acknowledgements. The present research is funded by International Center of Physics under grant number ICP.2022.09.

CRediT authorship contribution statement. Nguyen Dieu Linh: Methodology, Investigation, Data curation, Writing-original draft. Nguyen Thi Minh Hien: Validation, Writing-review & editing. Nguyen Thi Thuy Lieu: Methodology, Formal analysis. Tran Thi Kim Chi: Investigation, Formal analysis. Nguyen Xuan Nghia: Conceptualization, Supervision, Writing-review & editing.

Declaration of competing interest. The authors declare that they have no known competing financial interests or personal relationships that could have appeared to influence the work reported in this paper.

REFERENCES

1. Lee J. H., Song W. C., Yang K. J., Yoo Y. S. - Characteristics of the CdZnS thin film doped by indium diffusion, Thin Solid Films **416** (1-2) (2002) 184-189. doi:10.1016/s0040-6090(02)00702-2.

2. Zarkooshi A. A., Kaleli M. - Investigation of structural, morphological & optical properties of nanopowder CdZnS:Cu, Inorg. Chem. Commun. **127** (2021) 108508. doi:10.1016/j.inoche.2021.108508.
3. Nagamani K., Reddy M. V., Lingappa Y., Ramakrishna Reddy K. T., Miles R. W. - Physical Properties of $Zn_xCd_{1-x}S$ Nanocrytalline Layers Synthesized by Solution Growth Method, Int. J. Optoelectron. Eng. **2** (2) (2012) 1-4. doi: 10.5923/j.ijoe.20120202.01.
4. Pradhan N., Sarma, D. D. - Advances in Light-Emitting Doped Semiconductor Nanocrystals, J. Phys. Chem. Lett. **2** (21) (2011) 2818-2826. doi:10.1021/jz201132s.
5. Yadav I., Ahlawat, D. S. - Effect of dopant concentration on structural and optical properties of $Cd_{0.7}Zn_{0.3}S$ semiconducting nanocrystals, Mater. Sci. Eng. B **252** (2020) 114450. doi:10.1016/j.mseb.2019.114450.
6. Ahlawat D. S., Yadav I. - Optical, morphological and thermal investigation of Cu doped ternary semiconducting $Cd_{1-x}Zn_xS$:Cu nanomaterials, Opt. Mater. **119** (2021) 111377. doi:10.1016/j.optmat.2021.111377.
7. Tang A., Yi L., Han W., Teng F., Wang Y., Hou Y., Gao M. - Synthesis, optical properties, and superlattice structure of Cu(I)-doped CdS nanocrystals, Appl. Phys. Lett. **97**(3) (2010) 033112. doi:10.1063/1.3466664.
8. Srivastava B. B., Jana S., Pradhan N. - Doping Cu in Semiconductor Nanocrystals: Some Old and Some New Physical Insights, J. Am. Chem. Soc. **133**(4) (2011) 1007-1015. doi:10.1021/ja1089809.
9. Peng W. Q., Cong G. W., Qu S. C., Wang Z. G. - Synthesis and photoluminescence of ZnS:Cu nanoparticles, Opt. Mater. **29** (2-3) (2006) 313-317. doi:10.1016/ j.optmat.2005.10.003.
10. Singh S. B., Limaye M. V., Lalla N. P., Kulkarni S. K. - Copper-ion-induced photoluminescence tuning in CdSe nanoparticles, J. Lumin. **128**(12) (2008) 1909-1912. doi:10.1016/j.jlumin.2008.05.022.
11. Rajesh C., Phadnis C. V., Sonawane K. G., Mahamuni S. - Synthesis and optical properties of copper-doped ZnSe quantum dots, Phys. Scr. **90** (2015) 015803. doi:10.1088/0031-8949/90/1/015803.
12. Srivastava R. K., Pandey N., Mishra S. K. - Effect of Cu concentration on the photoconductivity properties of ZnS nanoparticles synthesized by co-precipitation method. Mater. Sci. Semicond, Process. **16**(6) (2013) 1659-1664. doi:10.1016/j.mssp.2013.06.009.
13. Liu B., Sharma M., Yu J., Shendre S., Hettiarachchi C., Sharma A., Yeltik A., Wang L., Sun H., Dang C., Demir H. V. - Light-Emitting Diodes with Cu-Doped Colloidal Quantum Wells: From Ultrapure Green, Tunable Dual-Emission to White Light, Small, (2019) 1901983. doi:10.1002/smll.201901983.
14. Chawla A. K., Singhal S., Nagar S., Gupta H. O., Chandra R. - Study of composition dependent structural, optical, and magnetic properties of Cu-doped $Zn_{1-x}Cd_xS$ nanoparticles, J. Appl. Phys. **108** (12) (2010) 123519. doi:10.1063/1.3524516.
15. Ouyang J., Ratcliffe C. I., Kingston D., Wilkinson B., Kuijper J., Wu X., Ripmeester J. A., Yu K. - Gradiently Alloyed $Zn_xCd_{1-x}S$ Colloidal Photoluminescent Quantum Dots Synthesized via a Noninjection One-Pot Approach, J. Phys. Chem. C **112** (13) (2008) 4908-4919. doi:10.1021/jp710852q.

16. Mansur A. A. P., Mansur H. S., Caires A. J., Mansur R. L., Oliveira, L. C. - Composition-Tunable Optical Properties of $Zn_xCd_{1-x}S$ Quantum Dot-Carboxymethylcellulose Conjugates: Towards One-Pot Green Synthesis of Multifunctional Nanoplatforms for Biomedical and Environmental Applications, Nanoscale Research Lett. **12** (2017) 443. doi:10.1186/s11671-017-2212-8.
17. Zhong X., Feng Y., Knoll W., Han M. - Alloyed $Zn_xCd_{1-x}S$ Nanocrystals with Highly Narrow Luminescence Spectral Width, J. Am. Chem. Soc. **125** (44) (2003) 13559-13563. doi:10.1021/ja036683a.
18. Madras G., McCoy B. J. - Distribution kinetics of Ostwald ripening at large volume fraction and with coalescence, J. Colloid Interf. Sci. **261** (2) (2003) 423-433. doi:10.1016/s0021-9797(03)00129-2.
19. Thang P. V., Tuyen H. V., Quang V. X., Lieu N. T. T., Thanh N. T., Nghia N. X. - Detection of luminescence centers in colloidal $Cd_{0.3}Zn_{0.7}S$ nanocrystals by synchronous luminescence spectroscopy, Commun. Phys. **30** (2) (2020) 181-187. doi:10.15625/0868-3166/30/2/13819.
20. Li J., Xia J. B. - Exciton states and optical spectra in CdSe nanocrystallite quantum dots, Phys. Rev. B **61** (23) (2000) 15880-15886. doi:10.1103/physrevb.61.15880.
21. Jasieniak J., Bullen C., van Embden J., Mulvaney P. - Phosphine-Free Synthesis of CdSe Nanocrystals, J. Phys. Chem. B **109** (44) (2005) 20665-20668. doi:10.1021/jp054289o.
22. Wang L., Jiang Y., Wang C., Wang W., Cao B., Niu M., Qian, Y. - Composition-controllable synthesis and optical properties of non-integral stoichiometry compound $Zn_xCd_{1-x}S$ nanorods, J. Alloys Compd. **454** (1-2) (2008) 255-260. doi:10.1016/j.jallcom.2006.12.046.
23. Chen Z., Tian Q., Song Y., Yang J., Hu J. - One-pot synthesis of $Zn_xCd_{1-x}S$ nanocrystals with tunable optical properties from molecular precursors, J. Alloys Compd. **506** (2) (2010) 804-810. doi:10.1016/j.jallcom.2010.07.075
24. Heitz R., Guffarth F., Mukhametzhanov I., Grundmann M., Madhukar A., Bimberg D. - Many-body effects on the optical spectra of InAs/GaAs quantum dots, Phys. Rev. B **62** (24) (2000) 16881-16885. doi:10.1103/physrevb.62.16881.
25. Nowak A. K., Gallardo E., van der Meulen H. P., Calleja J. M., Ripalda J. M., González L., González Y. - Band-gap renormalization in $InP/Ga_xIn_{1-x}P$ quantum dots, Phys. Rev. B **83** (24) (2011) 245447. doi:10.1103/physrevb.83.245447.